Precursor Film Mediated Thermocapillary Motion of Low Surface Tension Microdroplets

Teshima, Hideaki
Department of Aeronautics and Astronautics, Kyushu University

Misra, Sirshendu
Micro & Nano-Scale Transport Laboratory, University of Waterloo

Takahashi, Koji
Department of Aeronautics and Astronautics, Kyushu University

Mitra, Sushanta K
Micro & Nano-Scale Transport Laboratory, University of Waterloo

出版情報：Langmuir. 36 (19), pp.5096-5105, 2020-05-19. American Chemical Society : ACS
バージョン：
権利関係：

Precursor Film Mediated Thermocapillary Motion of Low Surface Tension Microdroplets

Hideaki Teshima[†, ‡], *Sirshendu Misra*[§], *Koji Takahashi*[†,‡], *Sushanta K. Mitra*[*,§]

[†] Department of Aeronautics and Astronautics, Kyushu University, Nishi-Ku, Motooka 744 Fukuoka 819-0395, Japan

[‡] International Institute for Carbon-Neutral Energy Research (WPI-I2CNER), Kyushu University, Nishi-Ku, Motooka 744 Fukuoka 819-0395, Japan

[§] Micro & Nano-Scale Transport Laboratory, Waterloo Institute for Nanotechnology, Department of Mechanical and Mechatronics Engineering, University of Waterloo, Waterloo, 200 University Avenue West, Waterloo, Ontario N2L 3G1, Canada

ABSTRACT

In contrast to microdroplet condensation with high contact angles, the one with low contact angles remains unclear. In this study, we investigated dynamics of microdroplet condensation of low surface tension liquids on two flat substrate surfaces by using reflection interference confocal microscopy. Spontaneous migration towards relatively larger droplets was first observed for the microdroplets nucleated on hydrophilic quartz surface. The moving microdroplets showed a contact angle hysteresis of ~0.5 °, which is much lower than the values observed on typical flat

substrates and is within the range observed on slippery lubricant-infused porous surfaces. Because the microdroplets on hydrophobic polydimethylsiloxane surface did not move, we concluded that the ultrathin precursor film is formed only on the hydrophilic surface, which reduces a resistive force to migration. Also, reduced size of droplets promotes the thermocapillary motion, which is induced by a gradient in local temperature inside a small microdroplet arising due to the difference in size of adjacent droplets.

Introduction

Study of droplet condensation in microscale does not only contain scope for exploring a broad variety of fundamentally rich thermophysical processes (which often differs significantly from its macroscale counterpart) but also holds promising potential in a multitude of practical purposes including microscale heat exchangers and heat pipes, bearing extensive implication in electronic circuitry. On the fundamental side, several experimental results have shown that microdroplets exhibit significantly lower contact angles compared to those observed on the macroscale[1,2]. This may arise from line tension and/or pinning effect[3,4]; however, a definitive explanation of extremely low contact angle is still lacking. On the application side, microdroplet condensation plays a key role, especially in phase change heat transfer[5–9]. For example, condensed microdroplets with a diameter of less than 100 μm account for approximately 80 % of the total heat transfer of dropwise condensation[9–12] and thus quick and continuous nucleation and departure of microdroplets are required for effective heat transfer. Several attempts are made to facilitate continuous removal of these condensed microdroplets and subsequent recovery of nucleation sites. Superhydrophobic surfaces with nanofabricated roughness features[13–16] and slippery lubricant-infused porous

surfaces (SLIPS)[8,17,18] are two of them, which have garnered significant interest in recent past. However, ensuring long term durability of these surfaces remains challenging[11,17,19] for either of them. Therefore, to unveil the fundamental problems and optimize the microdroplet condensation in such applications, further understanding of the dynamics of condensed microdroplets based on detailed observations is indispensable.

To observe the dynamics of microdroplet condensation, environmental scanning electron microscopy (ESEM) has been widely used because of good spatiotemporal resolution[6,20,21]. Due to the provision of precisely controlling the internal vapor pressure and the temperature of the sample stage, ESEM can easily induce the water droplet condensation with a size range of sub-micrometer to micrometer[20–25]. However, ESEM has two drawbacks. One is that the specific conditions in the ESEM chamber, such as low vapor pressure and electron beam irradiation, can affect the properties of droplets[23,24,26]. The other is that the vapor available for droplet condensation is restricted to water. Reflection interference contrast microscopy (RICM) is an alternative and promising way to observe the dynamics of droplet condensation. RICM can provide interference patterns corresponding to droplet thickness, which are essential for understanding the dynamic behavior of microdroplet condensation. In addition, microdroplet condensation of low surface tension liquids can be observed because there is no restriction of liquids and pressure. However, such studies using RICM are rare[1,27–30], and thus the scientific endeavor on the characterization of microdroplet condensation of low surface tension fluids consisting of alcohol and refrigerant is relatively scarce.

In this study, we observed the microdroplet condensation of low surface tension liquids on two different surfaces with different surface energy, namely, quartz and polydimethylsiloxane (PDMS) using RICM. By constructing the profile of microdroplets from the experimentally captured

interference patterns, growth and dynamics of the droplets with extremely low contact angles (approximately 4 °) were investigated. We found that droplets which nucleated on hydrophilic quartz surface spontaneously moved to relatively larger droplets and merged, while droplets on hydrophobic PDMS surface did not move and coalesced only when the three-phase contact line touched to neighboring droplets. In addition, the moving droplets showed extremely low contact angle hysteresis, like droplets observed on SLIPS surfaces. From these results, we attribute the mobility of droplets to thermocapillary motion mediated by a very thin precursor film, which reduces the contact angle hysteresis yielding a resistive force for the movement. This motion of small microdroplets towards large ones could be explained by taking a condensation induced local gradient in temperature into consideration. We also estimated the temperature gradient of the substrate surface underneath small microdroplets from the force balance analysis of the pinned microdroplets. Consequently, the temperature gradient was 2.3 ± 1.1 K/mm, which is comparable to those used in the previous reports on thermocapillary motion[31,32]. The reported motion can be realized on flat featureless surfaces and it does not require the above-mentioned complex surface features for droplet movement, such as nanofabricated superhydrophobic surfaces and SLIPS. These results will extend our fundamental knowledge about microdroplet condensation and will be valuable not only for condensation heat transfer but also in the various engineering applications, such as droplet-based microfluidics[33–36], anti-icing[19,37–39], water harvesting[40–43], and self-cleaning surface[44–47].

Experimental

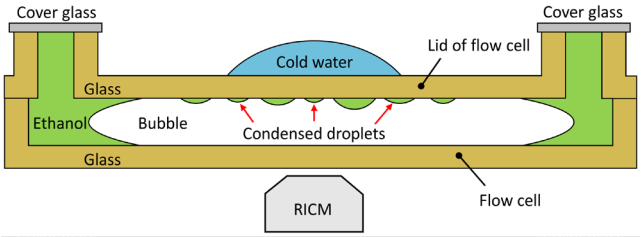

Figure 1. Schematic diagram of the experimental setup for RICM observation of microdroplet condensation. This image is not represented to scale for clarity.

The condensation experiments were carried out in a flow cell made of UV quartz (Type 49 Micro Demountable Flow Through Cell, Fireflysci Inc., NY). A schematic representation of the experimental set up is shown in Figure 1. First, 5 ml of test liquid was partially filled into the flow cell with the lid in place using a glass syringe. Then, 2-3 ml of air was infused into the liquid cell, which forms an air bubble. The liquid cell was slightly tilted to move the bubble up to the center of the liquid cell. The two inlets of the flow cell were then covered with glass coverslips to prevent evaporation of the test liquid. After putting the experimental setup on the observation stage of RICM, a drop of cold water (approximately 0.2 ml) was placed by a syringe on the top of the lid of the liquid cell to reduce the local temperature, resulting in the condensation of the test liquid vapor inside the liquid cell. Before the experiment, the syringe filled with 5 ml of deionized water was preserved in a refrigerator at a temperature of 4 ℃ for at least 1 hour. The cold droplet was then placed immediately after taking it out from the refrigerator. During the observation, we frequently added cold droplets on the top of the lid to sustain the condensation process. Even

without the addition of such liquid, condensation normally lasted for about 5 minutes. The room temperature was 22 ℃.

We have studied the condensation of two low surface tension liquids (i.e., ethanol and acetone) and a high surface tension liquid (i.e., deionized water). The ethanol and acetone are American Chemical Society reagent grade chemicals and purchased from Sigma Aldrich Canada Ltd. Deionized water was prepared using a water purifier (Milli-Q, 18.2 MΩ cm, MilliPore Sigma, Ontario, Canada). Droplet condensation on quartz was observed at the inner surface of the lid of the flow cell. For experiments on a PDMS surface, a thin slice of freshly prepared PDMS was utilized. Specifically, the PDMS substrates was prepared by thoroughly mixing the base reagent of the Sylgard 184 elastomer kit with the curing agent (Dow Inc.) in 10:1 weight ratio followed by degassing and subsequent curing at 60 ℃ for 12 hours. Young's modulus of the PDMS prepared by this procedure is 1.7 MPa[48]. The PDMS slice was placed on the inner surface of the lid of the flow cell by gently pressing it with a stainless steel tweezer, making use of the adhesive nature of PDMS. Water contact angles on quartz and PDMS surfaces are 31.7 ± 4 ° and 104.3 ± 2.5 °, respectively. Arithmetic mean surface roughness of the quartz and PDMS surface were measured by profilometer (P-6 stylus profiler, KLA Corp., vertical spatial resolution is 0.001 nm) and were 2.9 nm and 0.45 nm, respectively. Although both quartz and PDMS are non-conductive, static charges should not be present since the sample stage is grounded and humidity inside the liquid cell is very high. For every experiment, the microdroplets with various base radii were nucleated immediately after placing the cold water.

The condensation dynamics were captured by a custom-built LSM 800 (Carl Zeiss, Canada) RICM with a 10x objective lens with numerical aperture of 0.3 (EC Plan-Neofluar, Carl Zeiss, Canada). The observation area was scanned pixel-by-pixel using focused beam of monochromatic

laser with wavelength 488 nm. The incident light was collected through the pinhole with the size of 1 airy unit, which corresponds to an in-focus axial slice length of ~11 μm in our experiment. This pinhole improves signal to noise ratio by blocking out of focus light. The detected analog optical signal is then converted to a digital image using an inbuilt deconvolution algorithm. The dwell time at each pixel was less than 1 μs, which is necessary to have a satisfactory temporal resolution for capturing the dynamic behavior of droplet condensation.

In RICM setup, the incident light rays reflected from two interfaces, namely solid/liquid and liquid/air interfaces, interfere with one another. This interference results in the occurrence of bright and dark fringes depending on the difference in the light path. Difference in local height of the droplet between adjacent bright and dark fringes corresponds to $\lambda/(4n)$, where λ is the wavelength of the used laser source and n is the refractive index of the droplet. Using this interference pattern, we can construct the height profile of microdroplets. Detailed principle of generation of interference patterns is provided in Supporting Information (see Note 1). The shapes of deformed droplets caused by pinning of three-phase contact line were fitted by asymmetric quadratic function, enabling us to measure the contact angle hysteresis (see Supporting Information Note 2).

Results and Discussion

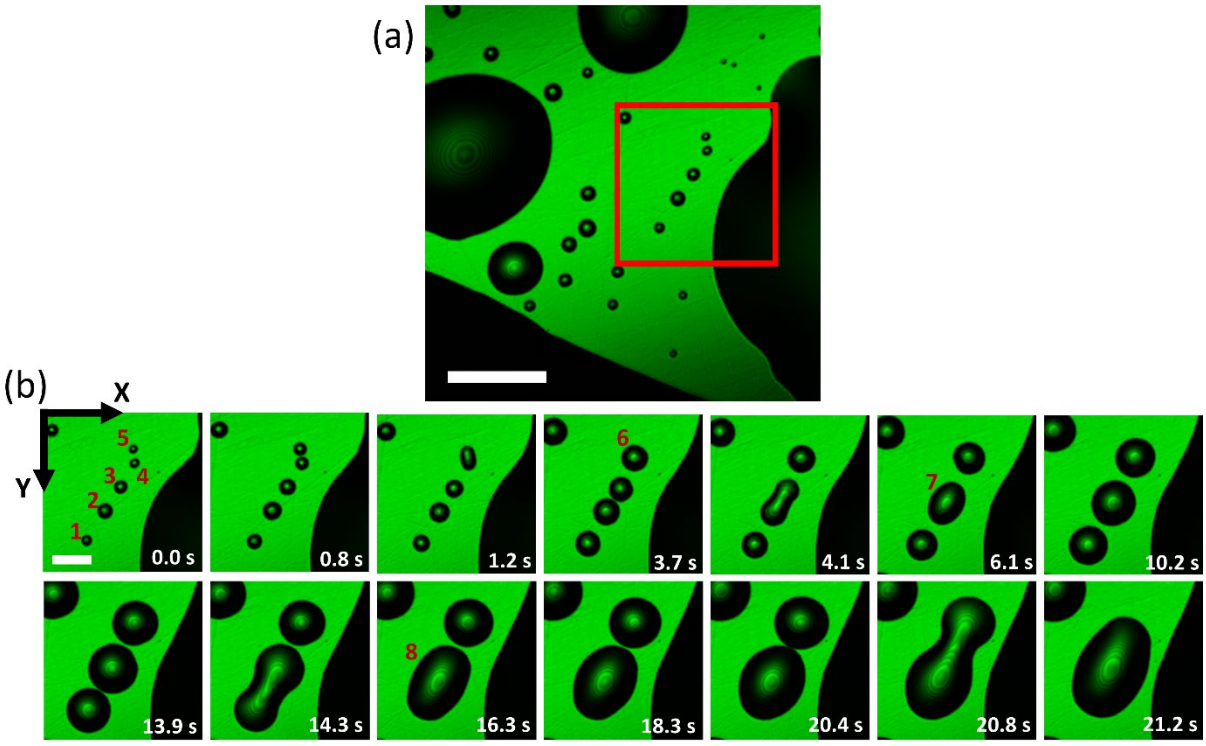

Figure 2. Ethanol microdroplet condensation on a PDMS surface. (a) The initial snap showing the entire observation area. The regions with dark edges are the nucleated microdroplets. (b) Time series demonstrating the dynamics of microdroplet condensation in the region indicated by a red square in (a). The video of this condensation experiment is available in Supporting Video S1. Scale bars are (a) 50 μm and (b) 20 μm, respectively.

Figure 2 shows condensation of ethanol microdroplets on a PDMS surface. The entire observation area is shown in Figure 2(a). Microdroplets of several different sizes nucleated instantaneously and appeared as black regions on the surface. Figure 2(b) shows the dynamics of droplet growth in the form of a time series in the region indicated by a red square in Figure 2(a). We observed the temporal evolution of 8 microdroplets (numbered 1-8 in the time series). As the

droplets grew in size, the contact line expanded in all directions. Eventually, small droplets coalesced and formed bigger droplets when their three-phase contact lines touched. The projection of the apex of the droplets on the contact surface (termed as the center of the droplets henceforth) remained almost stationary during the growth phase and it shifted only after merging with another neighboring droplet.

Note that we could not obtain the height of these microdroplets on PDMS surface because the region near the three-phase contact line did not show the interference patterns and appeared dark. This is because the rate of change in local height with respect to the base coordinate is so fast due to large contact angles that interference patterns appear very closely spaced, making the region dark.

It is known that a droplet on a soft substrate pulls the surface and makes a rim at the three-phase contact line, causing the self-pinning effect[49]. However, we did not observe such a deformation of the PDMS surface in our experiments. This is because Young's modulus of our PDMS is 1.7 MPa[48], which is higher than the values which cause non-negligible surface deformation[50]. Therefore, we assume that the self-pinning effect can be neglected on this PDMS surface.

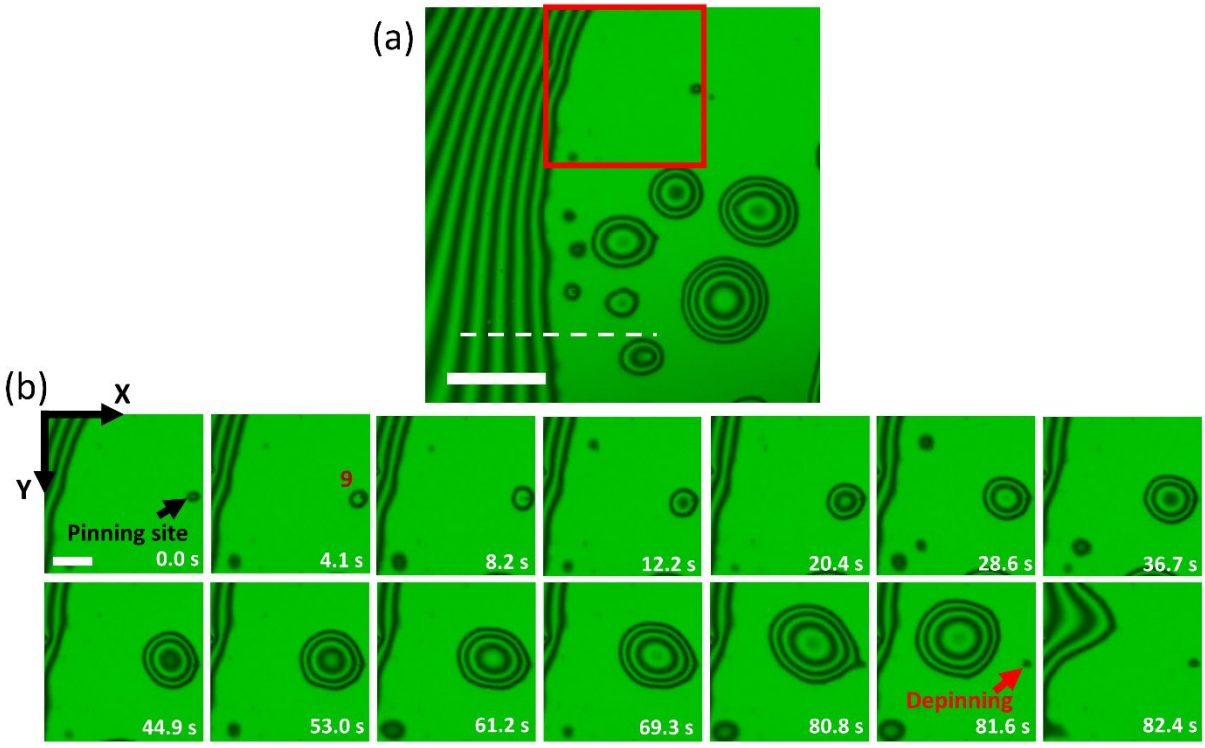

Figure 3. Ethanol microdroplet condensation on a quartz surface. (a) The initial snap showing the entire observation area containing the nucleated microdroplets. Normalized intensity profile along the white broken line is shown in Figure S2. (b) Time series demonstrating the dynamics of microdroplet condensation in the region indicated by a red square in (a). The video of this condensation experiment is available in Supporting Video S2. Scale bars are (a) 50 μm and (b) 20 μm, respectively.

Figure 3 shows an ethanol condensation experiment on a quartz surface. The entire observation area is shown in Figure 3(a). Interference patterns were observed throughout the nucleated microdroplets. This indicates that the contact angles of the microdroplets on the quartz are lower in comparison to those on the PDMS surface. Indeed, their contact angles and heights estimated from the constructed shapes were approximately 4 ° and less than 1 μm, which are very difficult

to be measured by normal optical microscopy due to the diffraction limit of light[51]. In Figure 3(b), temporal evolution of a microdroplet numbered 9 was tracked from its nucleation. The droplet was nucleated and pinned at an impurity indicated by a black arrow. During its growth, the center of the droplet clearly shifted to the left side. At 81.6 seconds, the three-phase contact line was eventually depinned from the impurity, as indicated by the red arrow. After the depinning, the microdroplet immediately moved to the left side and then merged with a bigger droplet. This indicates that a driving force is acting on the droplet and makes it move towards the left side.

Wayner's group has also observed droplet condensation of ethanol on a glass surface[28–30]. However, they reported that no significant flow from the small droplet towards the large droplet was observed and the spontaneous flow between them occurred only when three-phase contact lines comes into contact with each other[30], while in our experiments we observed spontaneous movement of small microdroplets towards big ones even without coalescence and merging of contact lines, as shown in the snap corresponding to 81.6 seconds in Figure 3(b). This may be because they could not find the phenomenon due to the short time scale of their observation (a few seconds) compared to that of the spontaneous movement of the microdroplets (several ten seconds).

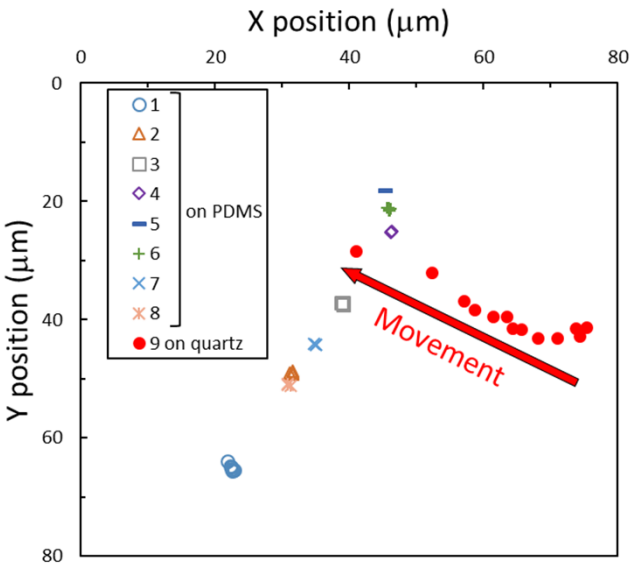

Figure 4. Scatter plot of center positions of ethanol droplets nucleated on PDMS and quartz surfaces. The numbers in legends correspond to droplet numbers shown in Figures 2(b) and 3(b).

In Figure 4, we tracked the center positions of the aforementioned 9 microdroplets. The base plane of the droplet is defined to be the XY plane and the top left corner of the time series images shown in Figure 2(b) and 3(b) was chosen as the origin of the coordinate system. The center positions of the microdroplets on the PDMS surface (number 1-8) almost overlapped. In contrast, the center position of the microdroplet on the quartz surface clearly shifted by around 40 μm towards left. This result indicates that low surface tension microdroplets nucleated on a surface with low surface energy remained almost stationary until they coalesced, while the microdroplets of the same liquid showed a mobile nature when they nucleated on a high energy surface. The mobility of nucleated microdroplets was also observed when we used the acetone as a low surface tension liquid (shown in Supporting Video S3). However, when we conducted water condensation on the quartz surface, the nucleated microdroplets did not move and showed the similar tendency as those observed on the PDMS surface (shown in Supporting Video S4). These results are an

unambiguous indication that the spontaneous movement is realizable exclusively for a combination of low surface tension liquid and high surface energy solid surface.

To investigate the mechanism behind the motion of low surface tension microdroplets on high energy surface, we analyzed another instance of ethanol condensation on the quartz surface as shown in Figure 5. Several small ethanol microdroplets with different base radii were nucleated in the center of the observation area. In addition, there are two large droplets in the left and right sides of the observation area. The trajectory of the center positions of the droplets in the left and right sides are shown by red and yellow arrows, respectively. It was found that the microdroplets in the left side of the observation area moved to the big droplet in the left, while the droplets on the right side approached and merged with the big droplet present on the right edge. From this observation, it is obvious that small droplets moved towards a bigger droplet close to them and not just towards a direction. It is to be emphasized that only the small microdroplets moved towards relatively large droplets and not vice versa. The migration of small droplets towards the nearest large droplet has been reported on SLIPS surfaces[8]. Sun and Weisensee explained that the mechanism of the migration is that the broad lubricant meniscus around a large droplet causes a difference in the inclination of the lubricant meniscus between the proximal and distal sides of nearby small droplets, resulting in a driving force towards the large droplet. In our case, however, we cannot explain the spontaneous movement of small droplets in the same manner because there are no such menisci around the droplets.

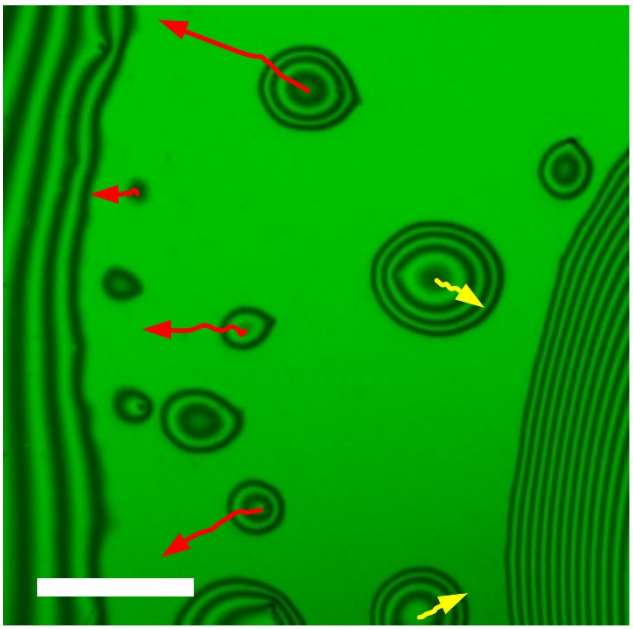

Figure 5. Trajectory of mobile ethanol droplets on the quartz surface. Red and yellow arrows track the center positions of mobile droplets. Scale bar is 50 μm. The video of this experiment showing the motion of the droplets is available in Supporting Video S5.

As a mechanism behind the movement, a vapor mediated movement on high energy surfaces can be considered[52–56]. For example, Cira et al. reported that two component droplets such as propylene glycol and water deposited on clean glass cause the motion of neighboring droplets over a distance, which is attributed to differential evaporation induced local imbalance in surface tension and consequent Marangoni flow[52]. Their system is clearly different from ours with only single test liquid. However, the motion of pure droplets, which is more similar to our system, has been theoretically and experimentally reported[53–55]. They proposed that, even in the absence of Marangoni effect, motion of pure droplets can be realized by a gradient in evaporation rate, which makes the droplets move from the high evaporation side to the low evaporation side. This is because a replenishing flow inside the droplet towards the high evaporation side pushes it towards

the opposite, high evaporation side by viscous friction from the substrate (Vapor-gradient mechanism)[55]. However, they experimentally observed the movement of bigger droplets towards small droplets as well[54], while we only observed that the small droplets moved towards big ones. Another definite difference is that the previously reported movements were only observed during evaporation. We also investigated evaporation of acetone droplets on the quartz surface and confirmed that the microdroplets did not move during evaporation (shown in Supporting Video S6). This may be because that the sizes of microdroplets in our study are much smaller than those of previous reports (~ several mm), reducing the difference in vapor between proximal and distal side of the droplets.

We also consider the effect of vapor for the droplet motion during condensation based on Sadafi et al.'s theory[55]. They proposed that there are two vapor-induced mechanisms that affect the interaction between two evaporating pure droplets; (i)Vapor-gradient mechanism as mentioned above and (ii)Vapor-induced temperature gradient mechanism that decreases local temperature at higher evaporation side (i.e. distal side) by latent heat, leading to thermocapillary motion away from the other droplet. Vapor also should affect the motion of microdroplets during condensation in a similar manner. For simplification, although there are several droplets in our observation, we consider the motion of two droplets. In regard to (i)Vapor-gradient mechanism, since the vapor near the proximal side is used for condensation of two droplets, the vapor influx to each droplet may become smaller at the proximal side than that at the distal side. Therefore, a replenishing flow will go into the proximal side, pushing the droplet towards the opposite (distal) direction. Therefore, the viscous force from the mechanism (i) will act as a resistance to the observed movement of smaller droplets towards large ones. On the other hand, the thermocapillary force induced by the mechanism (ii) enhances the droplet motion towards the other droplet since the

local temperature rise by condensation at the distal side is higher than that at the proximal side. In our experiments, the effect of (i) is not dominant because we observed the motion of the droplets towards the other ones, not the opposite direction. In contrast, the thermocapillary motion from the mechanism (ii) helps the droplets to move towards the other ones.

From the above discussions, we conclude that the underlying mechanism behind the droplet motion that we observed here is different from the vapor-gradient mechanism.

In addition, we also rule out the possible mechanism from the capillary pressure. If we assume that a fluid can flow inside the precursor film (or a suddenly formed liquid tunnel), mass transfer derived from the difference in Laplace pressure between large and small droplets occurs. In such a case, however, the movement of small droplets towards large droplets will not occur since viscous drag acts in the opposite direction to the flow. In addition, the moving droplets clearly increased their volume although the smaller droplets should become smaller and eventually disappear in case of a capillary pressure driven mass transfer process. Therefore, the capillary pressure cannot explain our observation results.

In our experiments, the moving microdroplets showed very low contact angle hysteresis (defined as the difference between the maximum and minimum contact angles measured for a single droplet). In Figure 3(c), the moving droplet at 81.6 seconds showed a contact angle hysteresis of approximately 0.5 °, which is much lower than the ones observed for macroscopic droplets (20-50°)[57] and is within the typical hysteresis range observed on slippery lubricant-infused porous (SLIPS) surfaces (< 3 °)[18]. Based on these observations, we conclude that vapor of low surface tension liquid adheres to high energy surface and forms an ultrathin liquid film during condensation, which has been called film-like condensate[58] or precursor film[59]. Our results indicate that the precursor film works as a lubricant layer and thus decreases the resistance for droplet

movement. It is known that a lubricant on SLIPS surfaces also works in a similar manner to the precursor film, although there are two significant difference; the precursor film component is that of fluid, while it is the lubricant oil in the case of SLIPS; The droplets in our experiments just sit on the precursor film, while the droplets on lubricant film can be encapsulated within the lubricant or create a rim at the three-phase contact line. Such encapsulation or the rim sometimes act opposing to coalescence[60].

To explain the movement of smaller microdroplets towards larger droplets, we propose the following mechanism. Temperature of microdroplets can increase in the process of condensation due to release of latent heat. However, the rate of temperature increment is low in large droplets due to the large heat capacity. In addition, thermal diffusion through the underlying substrate is also large due to large contact area with the quartz surface. Therefore, the temperature rise due to condensation is considered to be negligible for the large droplets. Rather, since the droplet acts as a thermal resistance, the substrate surface underneath the droplet attains a lower local temperature than that of the surrounding substrate surface[55]. In contrast, the temperature rise of small microdroplet becomes larger compared to that of large droplets because they have small heat capacity and contact area with the quartz surface. Therefore, a local temperature gradient is formed between the neighboring small and large droplets, causing a heat flow from the small droplet towards the bigger droplet. Essentially, the bigger droplet acts as a heat sink. This results in a local temperature gradient inside the small droplet where the edge of droplet closer to the bigger droplet has a lower local temperature than that of the edge away from it. It gives rise to a surface tension imbalance inside the small droplet, resulting in a thermocapillary motion towards the large droplet. Although such temperature profiles also appear on ethanol droplets on the PDMS surface and on water droplets on the quartz surface, they cannot move along the surface because of absence of the

precursor film, without which the thermocapillary force cannot overcome the resistance in motion arising because of direct droplet-substrate contact. It has been indeed reported that the contact angle hysteresis prevents the droplet from thermocapillary motion[31,32,61].

To validate this mechanism, we first provide a theoretical prediction of the presence or absence of the precursor film on quartz and PDMS surfaces. The existence of precursor film is determined by the sign of the difference in two Hamaker constants $A = A_{\mathrm{SL}} - A_{\mathrm{LL}}$ and the spreading coefficient $S = \gamma_{\mathrm{SV}} - \gamma_{\mathrm{SL}} - \gamma_{\mathrm{LV}}$[62], where γ is surface tension and the subscripts S, L, and V indicate the solid, liquid, and vapor, respectively. Here, A_{SL} can be expressed as $A_{\mathrm{SL}} \approx \sqrt{A_{\mathrm{SS}} A_{\mathrm{LL}}}$[63]. A_{SS} for quartz and PDMS surfaces are 6.5×10^{-20} J and 4.4×10^{-20} J and A_{LL} for water, ethanol and acetone are 3.7×10^{-20}, 4.2×10^{-20} J and 4.1×10^{-20} J, respectively[63,64]. Therefore, for all the cases we used in our experiments (i.e., quartz-water/ethanol/acetone and PDMS-ethanol combinations), the sign of A was positive. In addition, the positive and negative value of S corresponds to the wetting states, namely complete wetting and partial wetting. In addition to the water droplet on a quartz surface as shown in the experimental section, the ethanol droplet on a PDMS surface also showed the finite contact angles of 39 ± 1 °, indicating the negative sign of S. In contrast, the ethanol and acetone droplets spread completely on a quartz surface, and thus the sign of S is positive.

It has been reported that the precursor film appears when both the sign of A and S are positive, while it does not appear on the combination of positive A and negative S[62,65]. Therefore, this theoretical prediction indicates that the ethanol and acetone form the precursor films on the hydrophilic quartz surface while the PDMS surface has no liquid film, which is consistent with our assumption. The sign of A and S and the existence of precursor film are summarized in Table 1. We also theoretically predicted that the precursor films around large and small microdroplets spread sufficiently and connect to each other (see Supporting Information Note 3).

Table 1 Sign of the difference in two Hamaker constants A and spreading coefficient S, and the existence of precursor film.

Solid	Liquid	A	S	Precursor film
PDMS	Ethanol	Positive	Negative	No
Quartz	Water	Positive	Negative	No
Quartz	Ethanol	Positive	Positive	Yes
Quartz	Acetone	Positive	Positive	Yes

Unfortunately, we could not experimentally observe the precursor film using our RICM because the reflected signal received from such an ultrathin film is essentially indistinguishable from the background intensity (see Supporting Information Note 4). The precursor film has been observed by the methods, such as Brewster angle microscopy[66] and ellipsometry[67]. Indeed, the existence of ultrathin film during ethanol condensation on a quartz surface has been reported in a previous report[29].

Next, we provide a simplified theoretical framework to qualitatively explain the difference in temperature rise between large and small microdroplets. Let us take a microdroplet of volume V at time t. Let us say that the drop volume increases by ΔV due to condensation in a differential time interval Δt. The heat energy ΔQ released from condensation during this process is

$$\Delta Q = \rho \Delta V H \tag{1}$$

where ρ is the density of condensed liquid and H is the specific latent heat of condensation. Here, if we consider that the timescale Δt is sufficiently small, we can assume that the heat generated due to droplet condensation is used solely to increase the temperature of the droplet by ΔT. We use $\Delta t = 0.1$ ms for the estimation, which is much shorter than the time scale of the conduction[20]

through the quartz, $t_{\text{conduction}} \approx L^2/\alpha \approx 3$ ms, where $L = 2$ mm and $\alpha = 1.4 \times 10^{-3}\, m^2/s$ are the thickness and thermal diffusivity of a quartz, respectively. By considering the energy balance, we obtain

$$\Delta T = \frac{H}{C_p}\frac{\Delta V}{V + \Delta V} \tag{2}$$

where C_p is the specific heat capacity. The volume V can be geometrically expressed as

$$V = \frac{1}{3}\pi r^3 \frac{(2+\cos\theta)(1-\cos\theta)^2}{\sin^3\theta} \tag{3}$$

where r and θ are the mean base radius and contact angle of a microdroplet, respectively. Figure 6(a) shows a plot of contact angles of an ethanol droplet on the quartz surface as a function of mean base radius. It was found that the contact angles were almost constant at ~4 ° and independent on the mean base radius. Therefore, by differentiating Eq. (3) by the time t under the assumption that contact angle is constant, we obtain

$$\frac{dV}{dt} = \pi r^2 \frac{(2+\cos\theta)(1-\cos\theta)^2}{\sin^3\theta}\frac{dr}{dt} \tag{4}$$

For a sufficiently small Δt, ΔV can be expressed as $\Delta V = \frac{dV}{dt}\Delta t$. Therefore, Eq. (2) can be written as

$$\Delta T = \frac{\mathrm{H}}{\mathrm{C_p}}\frac{3\Delta \mathrm{t}\frac{dr}{dt}}{r+3\Delta \mathrm{t}\frac{dr}{dt}} \tag{5}$$

Experimentally obtained values of base radii r of the ethanol microdroplet at different time t are plotted in Figure 6(b). A linear fit between r and t clearly represented the experimentally obtained plot reasonably well (R-square value of 0.9929). Therefore, we can assume $\frac{dr}{dt}$ to be constant for our analysis. In addition, the value of $\frac{dr}{dt}$ shown in Figure 6(b) was 0.15. Using the experimentally obtained values in Eq. (5), we finally obtained a theoretical trend for variation of

ΔT with mean base radius r, as shown in Figure 6(c). Note that this equation (5) is derived to qualitatively discuss the trend of the temperature difference between small and large droplets.

From the trend in Figure 6(c), we can conclude that the smaller microdroplets experience a higher temperature increment during condensation than that of the bigger ones. This result is in agreement with our assumption that the temperature rise of small microdroplets becomes larger compared to that of large droplets. Large droplets have a higher heat dissipation to the substrate (acting as a local heat sink) and therefore temperature rise becomes much smaller, while the temperature of small microdroplets becomes high due to small heat dissipation. Therefore, within the small microdroplet, a local temperature gradient is established between the edge closer to the bigger droplet and the edge away from it, resulting in thermocapillary motion.

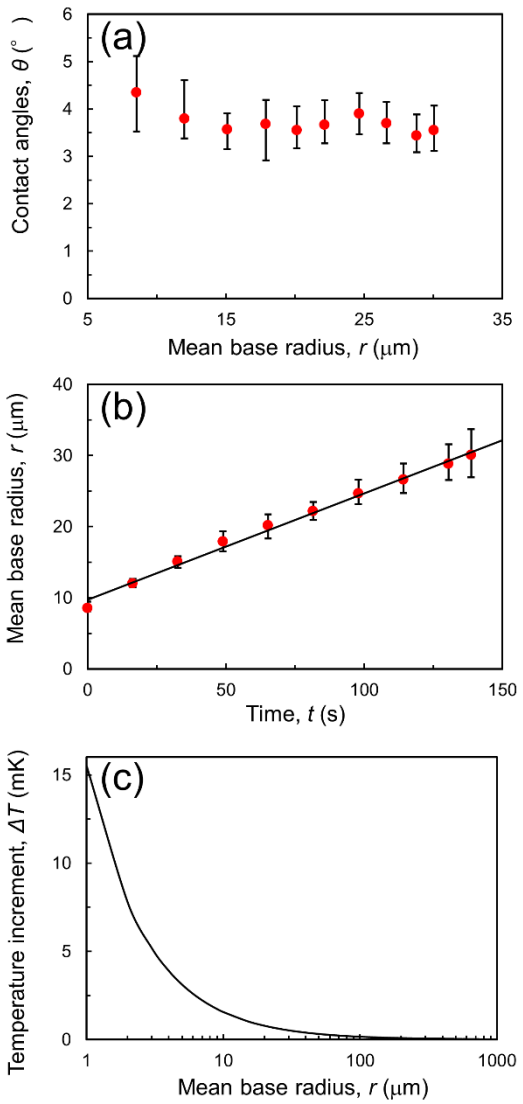

Figure 6. Analysis of the dynamics of growth of an ethanol microdroplet on a quartz surface. (a) Contact angle θ vs mean base radius r of an ethanol droplet nucleated on a quartz surface. (b) Mean base radius r vs time t. A slope of fitting line in (b) is $\frac{dr}{dt} = 0.15$ and R-square value is 0.9929. Upper and lower limits of error bars shown in (a) and (b) indicate maximum and minimum values obtained by our analysis. (c) Theoretical trend of temperature increment ΔT during $\Delta t = 0.1$ ms as a function of base radius. The material parameters of ethanol are $H = 838$ J/g, $C_{\mathrm{p}} = 2.42$ J/gK, and an averaged value of the contact angles $\theta = 3.7$ °.

From the force balance of the pinned ethanol microdroplets, we quantitatively estimate the driving force responsible for the spontaneous movement and the temperature gradient inside small microdroplets. On the pinned microdroplets as shown in Figure 3(b), hydrodynamic force induced by the thermocapillary flow, $F_{\mathrm{h}} = \frac{\partial \gamma_{\mathrm{LV}}}{\partial T}\frac{\partial T}{\partial x}\frac{\pi r^2}{2}$ and the force at three-phase contact line arising from the surface tension, $F_{\mathrm{cl}} = \frac{\partial \gamma_{\mathrm{LV}}}{\partial T}\frac{\partial T}{\partial x}\pi r^2 \cos\theta$ act in the direction of the larger droplet[31,68]. In addition, the pinning force, $F_{\mathrm{P}} = \frac{\Delta S\gamma}{h}$ works at the pinning site (i.e., the impurity) in the opposite direction[69]. Here, h is the length of the neck pulled up by F_{h} and F_{cl}, and $\Delta S\gamma$ is the change in surface energy of the droplet, where $\Delta S = S_{\mathrm{pulled}} - S_{\mathrm{unpulled}}$ is the difference in the surface area between the pulled and unpulled microdroplets, which can be estimated from the experimental data. Because the pinned droplet is static, these forces should be in balance. By assuming that the base area is a circle, the force balance can be written as follows

$$\frac{\partial \gamma_{\mathrm{LV}}}{\partial T}\frac{\partial T}{\partial x}\frac{\pi r^2}{2}(1 + 2\cos\theta) = \frac{\Delta S\gamma}{h} \qquad (6)$$

The rate of change of the ethanol-vapor interfacial tension with temperature $\frac{\partial \gamma_{\mathrm{LV}}}{\partial T}$ was estimated as 6.37×10^{-5} N/(m*K) from literature[70]. Since the small microdroplets start to move immediately after depinning, the values of the pinning force F_{P} at the maximal extension of the neck, as shown in the 80.8 seconds of Figure 3(b), should be almost the same as the driving force on the moving microdroplet. Hence, from several microdroplets just before the depinning, the driving force was estimated as 208 ± 50 pN. The spontaneous movement despite extreme smallness of the forces is attributed to the reduction of resistive force from the solid surface by formation of the precursor film.

From the equation (6), the temperature gradient inside small microdroplets along the direction of the spontaneous movement $\frac{\partial T}{\partial x}$ was also estimated as 2.3 ± 1.1 K/mm, which is comparable to the value typically used to induce the thermocapillary motion[31,32]. However, although the microdroplets on a PDMS surfaces also experience the similar temperature gradient, the droplets did not move. This is because there is the critical radius below which the droplets cannot move even on the thermal-gradient surface due to the contact angle hysteresis[31,32,61]. For example, Pratap et al. reported the critical radius of decane droplets on a PDMS surface with the temperature gradient of 1.05 - 2.77 K/mm is approximately 0.27 mm[31]. Therefore, it can be considered that the ethanol microdroplets on a PDMS surface did not move because their sizes were smaller than the critical radius induced by the contact angle hysteresis. In contrast, the ethanol microdroplets on the quartz surface were spontaneously moved even when the base radii of them are less than 20 μm, which are much smaller than the typical critical radius[31,32,61]. This indicates that the critical radius of the ethanol droplets on the hydrophilic quartz surface was significantly decreased because the precursor film reduced the resistive force exerted from the quartz surface, resulting in the extremely small contact angle hysteresis (~ 0.5 °).

In our experiments, the minimum base radius at which the spontaneous movement occurred was approximately 3.5 μm. We noted that the spontaneous movement takes place when the neck of the droplets that is pulled by the pinning sites becomes unstable and pinches off, as shown in Figure 3(b). The neck becomes unstable as the size of the droplet increases and/or the size of the pinning site decreases[69]. Therefore, it can be considered that larger droplets are more likely to detach on the surface and the minimum base radius for the spontaneous movement becomes smaller on smoother and cleaner surfaces.

Lastly, we analyzed the migration velocity of the depinned microdroplet shown in the frame at 81.6 seconds in Figure 3(b) and quantitatively compared with the theoretical value. Pratap et al. reported that the temperature-induced induced motion of the droplet can be modeled as a quasi-steady process and the migration velocity V can be written as follows[31]

$$V = \frac{r\frac{\partial \gamma_{\mathrm{LV}}}{\partial T}\frac{\partial T}{\partial x}(1+2\cos\theta)}{12\mu[g(\theta,1-\epsilon)-g(\theta,0)]} \tag{7}$$

where

$$g(\theta,\zeta) = \cot\theta\left[1-\ln\left(\sqrt{\mathrm{cosec}^2\,\theta-\zeta^2}-\cot\theta\right)\right]-\sqrt{\mathrm{cosec}^2\,\theta-\zeta^2} \tag{8}$$

$\mu = 1.2\times10^{-3}\ Pa\cdot s$ is the viscosity of ethanol and ϵ is a constant value that is defined as $\epsilon = L_{\mathrm{s}}/r$, where $L_{\mathrm{s}} = 0.5$ nm is a cutoff length value of the order of molecular dimensions, introduced solely to avoid mathematical singularity. By applying the equation (7) to the depinned droplet, the migration velocity can be estimated. Accordingly, the value was approximately 4.2 μm/s. On the other hand, the experimental value of the migration velocity of the same microdroplet (defined as the rate of the change of the center position with respect to time) was approximately 12.7 μm/s, which is higher than the theoretical value. This may be because the droplet still does not reach the quasi-steady condition since the sudden depinning breaks the balance of the forces working on the droplet, resulting in sudden acceleration of the droplet. Further quantitative characterization of the spontaneous motion remains an interesting topic for future studies, but beyond the scope of the present paper that focuses on the mechanism of the spontaneous motion.

Conclusions

In this work, we report experimental observation of condensation of microdroplets with extremely low contact angles. We found that contact angles of ethanol microdroplets condensed

on a hydrophilic quartz surface were constant (approximately 4 °) and did not depend on the base radius. The small microdroplets spontaneously moved to relatively large droplets during condensation. Although we conducted the microdroplet condensation by using high surface tension liquid (i.e. deionized water) and a hydrophobic PDMS surface, this movement occurred only when we used the combination of a low surface tension liquid and a hydrophilic surface. In addition, the moving droplets showed extreme low contact angles hysteresis. From these results, we attributed this motion to two factors, namely, formation of an ultrathin precursor film and a gradient in local temperature inside the small microdroplet caused by the difference in adjacent droplet sizes. The local temperature gradient causes thermocapillary effect and thus makes the small microdroplets move towards the large droplet close to them. The presence of the ultrathin precursor film underneath the nucleated droplets facilitates the motion by reducing the resistive force to migration. The driving force for the migration and the temperature gradient inside a small microdroplet were quantitatively calculated from the force balance of the pinned microdroplets. The extremely small driving force and the onset of the movement of the microdroplets with the very small base radius are the incontrovertible evidence of the existence of precursor film. These results will extend our fundamental knowledge about microdroplet condensation and will be valuable for condensation heat transfer.

ASSOCIATED CONTENT

Supporting Information

The Supporting Information is available free of charge.

Principle of generation of interference patterns, fitting of asymmetric shape of condensed microdroplets, lateral extension of precursor film, and background noise of reflected light in RICM observation (PDF)

Condensation of ethanol microdroplets on a PDMS surface (MP4)

Condensation of ethanol microdroplets on a quartz surface (MP4)

Condensation of acetone microdroplets on a quartz surface (MP4)

Condensation of water microdroplets on a quartz surface (MP4)

Condensation of ethanol microdroplets on a quartz surface_2 (MP4)

Evaporation of ethanol microdroplets on a quartz surface (MP4)

AUTHOR INFORMATION

Corresponding Author

∗ E-mail: skmitra@uwaterloo.ca.

Notes

The authors declare no competing financial interest.

ACKNOWLEDGMENTS

This work was partially supported by S.K.M's Discovery Grant (RGPIN-2019-04060) from Natural Sciences and Engineering Research Council (NSERC), Canada and by K.T's JST CREST

Grant No. JPMJCR18I1 and a Grant-in-Aid for JSPS Research Fellow No. JP18J11880, Japan. S. M. additionally acknowledges financial support from Waterloo Institute for Nanotechnology, University of Waterloo in the form of Nanofellowship 2018. We thank Dr. Kiran Raj M for support with surface profilometry. We also thankfully acknowledge Dr. Enrique Wagemann for helpful scientific discussion, Yuko Nishizawa for valuable suggestion about asymmetric quadratic function and Dr. Mizuki Tenjimbayashi for helpful suggestions during designing the 3D cover art.

REFERENCES

(1) Stöckelhuber, K. W.; Radoev, B.; Schulze, H. J. Some New Observations on Line Tension of Microscopic Droplets. *Colloids Surfaces A Physicochem. Eng. Asp.* **1999**, *156*, 323–333.

(2) Heim, L. O.; Bonaccurso, E. Measurement of Line Tension on Droplets in the Submicrometer Range. *Langmuir* **2013**, *29*, 14147–14153.

(3) Zhang, H.; Chen, S.; Guo, Z.; Liu, Y.; Bresme, F.; Zhang, X. Contact Line Pinning Effects Influence Determination of the Line Tension of Droplets Adsorbed on Substrates. *J. Phys. Chem. C* **2018**, *122*, 17184–17189.

(4) Lohse, D.; Zhang, X. Surface Nanobubbles and Nanodroplets. *Rev. Mod. Phys.* **2015**, *87*, 981–1035.

(5) Daniel, S.; Chaudhury, M. K.; Chen, J. C. Fast Drop Movements Resulting from the Phase Change on a Gradient Surface. *Science (80-.).* **2001**, *291*, 633–636.

(6) Miljkovic, N.; Wang, E. N. Condensation Heat Transfer on Superhydrophobic Surfaces. *MRS Bull.* **2013**, *38*, 397–406.

(7) Chu, F.; Wu, X.; Zhu, B.; Zhang, X. Self-Propelled Droplet Behavior during Condensation on Superhydrophobic Surfaces. *Appl. Phys. Lett.* **2016**, *108*, 194103.

(8) Sun, J.; Weisensee, P. B. Microdroplet Self-Propulsion during Dropwise Condensation on Lubricant-Infused Surfaces. *Soft Matter* **2019**, *15*, 4808–4817.

(9) Orejon, D.; Shardt, O.; Waghmare, P. R.; Kumar Gunda, N. S.; Takata, Y.; Mitra, S. K. Droplet Migration during Condensation on Chemically Patterned Micropillars. *RSC Adv.* **2016**, *6*, 36698–36704.

(10) Weisensee, P. B.; Wang, Y.; Qiang, H.; Schultz, D.; King, W. P.; Miljkovic, N. Condensate Droplet Size Distribution on Lubricant-Infused Surfaces. *Int. J. Heat Mass Transf.* **2017**, *109*, 187–199.

(11) Rose, J. W. Dropwise Condensation Theory and Experiment: A Review. *Proc. Inst. Mech. Eng. Part A J. Power Energy* **2002**, *216*, 115–128.

(12) Orejon, D.; Shardt, O.; Gunda, N. S. K.; Ikuta, T.; Takahashi, K.; Takata, Y.; Mitra, S. K. Simultaneous Dropwise and Filmwise Condensation on Hydrophilic Microstructured Surfaces. *Int. J. Heat Mass Transf.* **2017**, *114*, 187–197.

(13) Lafuma, A.; Quéré, D. Superhydrophobic States. *Nat. Mater.* **2003**, *2*, 457–460.

(14) Yan, X.; Zhang, L.; Sett, S.; Feng, L.; Zhao, C.; Huang, Z.; Vahabi, H.; Kota, A. K.; Chen, F.; Miljkovic, N. Droplet Jumping: Effects of Droplet Size, Surface Structure, Pinning, and Liquid Properties. *ACS Nano* **2019**, *13*, 1309–1323.

(15) Miljkovic, N.; Enright, R.; Nam, Y.; Lopez, K.; Dou, N.; Sack, J.; Wang, E. N. Jumping-Droplet-Enhanced Condensation on Scalable Superhydrophobic Nanostructured Surfaces. *Nano Lett.* **2013**, *13*, 179–187.

(16) Boreyko, J. B.; Chen, C. H. Self-Propelled Dropwise Condensate on Superhydrophobic Surfaces. *Phys. Rev. Lett.* **2009**, *103*, 184501.

(17) Anand, S.; Paxson, A. T.; Dhiman, R.; Smith, J. D.; Varanasi, K. K. Enhanced Condensation on Lubricant-Impregnated Nanotextured Surfaces. *ACS Nano* **2012**, *6*, 10122–10129.

(18) Lafuma, A.; Quéré, D. Slippery Pre-Suffused Surfaces. *Europhys. Lett.* **2011**, *96*, 56001.

(19) Kreder, M. J.; Alvarenga, J.; Kim, P.; Aizenberg, J. Design of Anti-Icing Surfaces: Smooth, Textured or Slippery? *Nat. Rev. Mater.* **2016**, *1*, 15003.

(20) Rykaczewski, K. Microdroplet Growth Mechanism during Water Condensation on Superhydrophobic Surfaces. *Langmuir* **2012**, *28*, 7720–7729.

(21) Yamada, Y.; Ikuta, T.; Nishiyama, T.; Takahashi, K.; Takata, Y. Droplet Nucleation on a Well-Defined Hydrophilic-Hydrophobic Surface of 10 Nm Order Resolution. *Langmuir* **2014**, *30*, 14532–14537.

(22) Anand, S.; Son, S. Y. Sub-Micrometer Dropwise Condensation under Superheated and Rarefied Vapor Condition. *Langmuir* **2010**, *26*, 17100–17110.

(23) Stelmashenko, N. A.; Craven, J. P.; Donald, A. M.; Terentjev, E. M.; Thiel, B. L. Topographic Contrast of Partially Wetting Water Droplets in Environmental Scanning Electron Microscopy N. *J. Microsc.* **2001**, *204*, 172–183.

(24) Rykaczewski, K.; Scott, J. H. J.; Fedorov, A. G. Electron Beam Heating Effects during Environmental Scanning Electron Microscopy Imaging of Water Condensation on Superhydrophobic Surfaces. *Appl. Phys. Lett.* **2011**, *98*, 093106.

(25) Miljkovic, N.; Enright, R.; Wang, E. N. Effect of Droplet Morphology on Growth Dynamics and Heat Transfer during Condensation on Superhydrophobic Nanostructured Surfaces. *ACS Nano* **2012**, *6*, 1776–1785.

(26) Méndez-Vilas, A.; Jódar-Reyes, A. B.; González-Martín, M. L. Ultrasmall Liquid Droplets on Solid Surfaces: Production, Imaging, and Relevance for Current Wetting Research. *Small* **2009**, *5*, 1366–1390.

(27) Sundberg, M.; Månsson, A.; Tågerud, S. Contact Angle Measurements by Confocal Microscopy for Non-Destructive Microscale Surface Characterization. *J. Colloid Interface Sci.* **2007**, *313*, 454–460.

(28) Wang, Y. X.; Plawsky, J. L.; Wayner, P. C. Optical Measurement of Microscale Transport Processes in Dropwise Condensation. *Microscale Thermophys. Eng.* **2001**, *5*, 55–69.

(29) Gokhale, S. J.; Plawsky, J. L.; Wayner, P. C.; DasGupta, S. Inferred Pressure Gradient and Fluid Flow in a Condensing Sessile Droplet Based on the Measured Thickness Profile. *Phys. Fluids* **2004**, *16*, 1942–1955.

(30) Wayner, P. C. Nucleation, Growth and Surface Movement of a Condensing Sessile Droplet Peter. *Colloids Surfaces A Physicochem. Eng. Asp.* **2002**, *206*, 157–165.

(31) Pratap, V.; Moumen, N.; Subramanian, R. S. Thermocapillary Motion of a Liquid Drop on a Horizontal Solid Surface. *Langmuir* **2008**, *24*, 5185–5193.

(32) Chen, J. Z.; Troian, S. M.; Darhuber, A. A.; Wagner, S. Effect of Contact Angle Hysteresis on Thermocapillary Droplet Actuation. *J. Appl. Phys.* **2005**, *97*, 014906.

(33) Teh, S. Y.; Lin, R.; Hung, L. H.; Lee, A. P. Droplet Microfluidics. *Lab Chip* **2008**, *8*, 198–220.

(34) Yan, Z.; Jin, M.; Li, Z.; Zhou, G.; Shui, L. Droplet-Based Microfluidic Thermal Management Methods for High Performance Electronic Devices. *Micromachines* **2019**, *10*, 1–16.

(35) Yang, C. G.; Xu, Z. R.; Wang, J. H. Manipulation of Droplets in Microfluidic Systems. *Trends Anal. Chem.* **2010**, *29*, 141–157.

(36) Garcia-Cordero, J. L.; Fan, Z. H. Sessile Droplets for Chemical and Biological Assays. *Lab Chip* **2017**, *17*, 2150–2166.

(37) Yamazaki, T.; Tenjimbayashi, M.; Manabe, K.; Moriya, T.; Nakamura, H.; Nakamura, T.; Matsubayashi, T.; Tsuge, Y.; Shiratori, S. Antifreeze Liquid-Infused Surface with High Transparency, Low Ice Adhesion Strength, and Antifrosting Properties Fabricated through a Spray Layer-by-Layer Method. *Ind. Eng. Chem. Res.* **2019**, *58*, 2225–2234.

(38) Wilson, P. W.; Lu, W.; Xu, H.; Kim, P.; Kreder, M. J.; Alvarenga, J.; Aizenberg, J. Inhibition of Ice Nucleation by Slippery Liquid-Infused Porous Surfaces (SLIPS). *Phys. Chem. Chem. Phys.* **2013**, *15*, 581–585.

(39) Kim, P.; Wong, T. S.; Alvarenga, J.; Kreder, M. J.; Adorno-Martinez, W. E.; Aizenberg, J. Liquid-Infused Nanostructured Surfaces with Extreme Anti-Ice and Anti-Frost Performance. *ACS Nano* **2012**, *6*, 6569–6577.

(40) Lalia, B. S.; Anand, S.; Varanasi, K. K.; Hashaikeh, R. Fog-Harvesting Potential of Lubricant-Impregnated Electrospun Nanomats. *Langmuir* **2013**, *29*, 13081–13088.

(41) Park, K. C.; Chhatre, S. S.; Srinivasan, S.; Cohen, R. E.; McKinley, G. H. Optimal Design of Permeable Fiber Network Structures for Fog Harvesting. *Langmuir* **2013**, *29*, 13269–13277.

(42) Seo, D.; Lee, C.; Nam, Y. Influence of Geometric Patterns of Microstructured Superhydrophobic Surfaces on Water-Harvesting Performance via Dewing. *Langmuir* **2014**, *30*, 15468–15476.

(43) Ju, J.; Bai, H.; Zheng, Y.; Zhao, T.; Fang, R.; Jiang, L. A Multi-Structural and Multi-Functional Integrated Fog Collection System in Cactus. *Nat. Commun.* **2012**, *3*, 1–6.

(44) Ganesh, V. A.; Raut, H. K.; Nair, A. S.; Ramakrishna, S. A Review on Self-Cleaning Coatings. *J. Mater. Chem.* **2011**, *21*, 16304–16322.

(45) Wong, T. S.; Kang, S. H.; Tang, S. K. Y.; Smythe, E. J.; Hatton, B. D.; Grinthal, A.; Aizenberg, J. Bioinspired Self-Repairing Slippery Surfaces with Pressure-Stable Omniphobicity. *Nature* **2011**, *477*, 443–447.

(46) Lu, Y.; Sathasivam, S.; Song, J.; Crick, C. R.; Carmalt, C. J.; Parkin, I. P. Robust Self-Cleaning Surfaces That Function When Exposed to Either Air or Oil. *Science (80-.).* **2015**, *347*, 1132–1135.

(47) Blossey, R. Self-Cleaning Surfaces - Virtual Realities. *Nat. Mater.* **2003**, *2*, 301–306.

(48) Johnston, I. D.; McCluskey, D. K.; Tan, C. K. L.; Tracey, M. C. Mechanical Characterization of Bulk Sylgard 184 for Microfluidics and Microengineering. *J. Micromechanics Microengineering* **2014**, *24*, 035017.

(49) Snoeijer, J. H.; Rolley, E.; Andreotti, B. Paradox of Contact Angle Selection on Stretched Soft Solids. *Phys. Rev. Lett.* **2018**, *121*, 68003.

(50) Pericet-Cámara, R.; Best, A.; Butt, H. J.; Bonaccurso, E. Effect of Capillary Pressure and Surface Tension on the Deformation of Elastic Surfaces by Sessile Liquid Microdrops: An Experimental Investigation. *Langmuir* **2008**, *24*, 10565–10568.

(51) Born, M.; Wolf, E. *Principles of Optics: Electromagnetic Theory of Propagation, Interference and Diffraction of Light*, 6th ed.; 2013.

(52) Cira, N. J.; Benusiglio, A.; Prakash, M. Vapour-Mediated Sensing and Motility in Two-Component Droplets. *Nature* **2015**, *519*, 446–450.

(53) Man, X.; Doi, M. Vapor-Induced Motion of Liquid Droplets on an Inert Substrate. *Phys. Rev. Lett.* **2017**, *119*, 044502.

(54) Wen, Y.; Kim, P. Y.; Shi, S.; Wang, D.; Man, X.; Doi, M.; Russell, T. P. Vapor-Induced Motion of Two Pure Liquid Droplets. *Soft Matter* **2019**, *15*, 2135–2139.

(55) Sadafi, H.; Dehaeck, S.; Rednikov, A.; Colinet, P. Vapor-Mediated versus Substrate-Mediated Interactions between Volatile Droplets. *Langmuir* **2019**, 1–9.

(56) Majhy, B.; Sen, A. K. Evaporation-Induced Transport of a Pure Aqueous Droplet by an Aqueous Mixture Droplet. *Phys. Fluids* **2020**, *32*.

(57) Quéré, D. Non-Sticking Drops. *Reports Prog. Phys.* **2005**, *68*, 2495–2532.

(58) Sheng, Q.; Sun, J.; Wang, Q.; Wang, W.; Wang, H. S. On the Onset of Surface Condensation: Formation and Transition Mechanisms of Condensation Mode. *Sci. Rep.* **2016**, *6*, 1–9.

(59) Popescu, M. N.; Oshanin, G.; Dietrich, S.; Cazabat, A. M. Precursor Films in Wetting Phenomena. *J. Phys. Condens. Matter* **2012**, *24*, 1–30.

(60) Boreyko, J. B.; Polizos, G.; Datskos, P. G.; Sarles, S. A.; Collier, C. P. Air-Stable Droplet Interface Bilayers on Oil-Infused Surfaces. *Proc. Natl. Acad. Sci. U. S. A.* **2014**, *111*, 7588–7593.

(61) Brzoska, J. B.; Brochard-Wyart, F.; Rondelez, F. Motions of Droplets on Hydrophobic Model Surfaces Induced by Thermal Gradients. *Langmuir* **1993**, *9*, 2220–2224.

(62) Brochard-Wyart, F.; di Meglio, J. M.; Quéré, D.; de Gennes, P. G. Spreading of Nonvolatile Liquids in a Continuum Picture. *Langmuir* **1991**, *7*, 335–338.

(63) Israelachvili, J. *Intermolecular and Surface Forces, 1985*, 3rd ed.; Academic Press, 2011.

(64) Drummond, C. J.; Chan, D. Y. C. Van Der Waals Interaction, Surface Free Energies, and Contact Angles: Dispersive Polymers and Liquids. *Langmuir* **1997**, *13*, 3890–3895.

(65) Bonn, D.; Eggers, J.; Indekeu, J.; Meunier, J. Wetting and Spreading. *Rev. Mod. Phys.* **2009**, *81*, 739–805.

(66) Ueno, I.; Hirose, K.; Kizaki, Y.; Kisara, Y.; Fukuhara, Y. Precursor Film Formation Process Ahead Macroscopic Contact Line of Spreading Droplet on Smooth Substrate. *J. Heat Transfer* **2012**, *134*, 1–4.

(67) Shoji, E.; Komiya, A.; Okajima, J.; Kubo, M.; Tsukada, T. Three-Step Phase-Shifting Imaging Ellipsometry to Measure Nanofilm Thickness Profiles. *Opt. Lasers Eng.* **2019**, *112*, 145–150.

(68) Brochard, F. Motions of Droplets on Solid Surfaces Induced by Chemical or Thermal Gradients. *Langmuir* **1989**, *5*, 432–438.

(69) Tan, B. H.; An, H.; Ohl, C.-D. Resolving the Pinning Force of Nanobubbles with Optical Microscopy. *Phys. Rev. Lett.* **2017**, *118*, 054501.

(70) Gonalves, F. A. M. M.; Trindade, A. R.; Costa, C. S. M. F.; Bernardo, J. C. S.; Johnson, I.; Fonseca, I. M. A.; Ferreira, A. G. M. PVT, Viscosity, and Surface Tension of Ethanol: New Measurements and Literature Data Evaluation. *J. Chem. Thermodyn.* **2010**, *42*, 1039–1049.

For Table of Contents Only